Eur. Phys. J. B **60**, 181–185 (2007)
DOI: 10.1140/epjb/e2007-00337-6

THE EUROPEAN PHYSICAL JOURNAL B

S-matrix poles close to thresholds in confined geometries

G. Cattapan[1,2,a] and P. Lotti[2,1]

[1] Dipartimento di Fisica "G. Galilei", Università di Padova, Via F. Marzolo 8, 35131 Padova, Italy
[2] Istituto Nazionale di Fisica Nucleare, Sezione di Padova, Via F. Marzolo 8, 35131 Padova, Italy

Received 25 June 2007 / Received in final form 23 October 2007
Published online 8 December 2007 –

Abstract. We have studied the behavior of the S–matrix poles near threshold for quantum waveguides coupled to a cavity with a defect. We emphasize the occurrence of both dominant and shadow poles on the various sheets of the energy Riemann surface, and show that the changes of the total conductivity near threshold as the cavity's width changes can be explained in terms of dominant to shadow pole transitions.

PACS. 73.63.Nm Quantum wires – 73.23.Ad Ballistic transport – 72.10.Fk Scattering by point defects, dislocations, surfaces, and other imperfections (including Kondo effect)

The analytic properties of the S–matrix have become by now one of the basic tools of modern scattering theory [1–3]. For multichannel scattering, each element of the S–matrix at a given total energy E depends upon the channel momenta

$$k_n = \sqrt{\frac{2\mu}{\hbar^2}\,(E-\epsilon_n)}, \tag{1}$$

where ϵ_n are the threshold energies, μ the mass of the scattered particle, and we have used non–relativistic kinematics, since this is the case we shall consider in this paper. Because of equation (1), if N coupled channels are taken into account, there are 2^N possible choices for the complex momenta k_n when the scattering matrix is analytically continued to complex values of E. The S–matrix has therefore to be considered on a Riemann surface with 2^N sheets, the thresholds ϵ_n being square–root branch points, with cuts which by general convention run in the positive direction of the real energy axis. From this point of view, the physical transition amplitudes are just the real–boundary values of the S–matrix elements, regarded as analytic functions of the complex energy E. The very existence and nature of the above threshold singularities can be inferred on the ground of general unitarity arguments [1]. For non–relativistic systems the analytic continuation of the physical S–matrix into the various sheets can be related to the possible boundary conditions one may choose for the solution of the Schrödinger equation [2,3]. On the physical sheet, one has exponentially decreasing waves for the bound states of the system, and asymptotically outgoing waves in all open channels at real energy; in correspondence to the bound states one finds poles of the S–matrix on the real energy axis. Singularities on other non–physical sheets correspond to non–physical boundary conditions, but are nevertheless amenable to a physical interpretation if they are close to the physical energy axis. Thus, for $\mathrm{Im}\, k_n < 0$ one imposes purely emissive boundary conditions, with outgoing waves in the corresponding channel which explode exponentially at large distances, whereas when $\mathrm{Im}\, k_n > 0$ the wave function decreases exponentially in the asymptotic region. The generalized eigenfunctions of the Schrödinger equation one gets in the former case are quite akin to the Gamow–Siegert wave functions for single–channel scattering [2–4]; the corresponding eigenvalues are complex, and appear as poles of the S–matrix elements, with the imaginary part proportional to the width of the associated resonant state. In addition to these "dominant" singularities, there may be also poles of the S–matrix on other unphysical sheets of the Riemann energy surface, far away from the physical region, which have been referred to as *shadow* poles [5]. The existence of these singularities has been established in [5] on the ground of the unitarity relations, analytically continued into the unphysical sheets of the energy Riemann surface, supplemented with general assumptions about the analyticity of the transition amplitudes. The possible role of shadow poles, and whether they may lead to observable effects in the physical transition amplitudes has been discussed over the years in the context of particle [6], nuclear [7] and atomic [8] physics, as well as in laser–induced multi-photon processes [9,10]. Their study is of particular relevance when the scattering process depends upon some tunable parameter; as this parameter is changed, the S–matrix poles move on the various sheets of the energy Riemann surface, and may pass a scattering threshold. In so doing, some shadow pole may approach the physical region, thereby becoming dominant, and

[a] e-mail: giorgio.cattapan@pd.infn.it

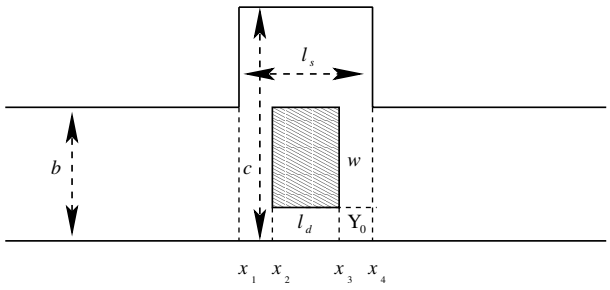

Fig. 1. A stubbed quantum waveguide of width b and infinite length, with a stub of width c and length l_s. The stub contains a defect with dimensions $w \times l_d$.

producing observable effects, whereas a previously dominant pole may retire to a less exposed position [3].

In this paper we would like to point out another situation, where shadow and dominant poles may exchange their roles, and give rise to non–trivial observable effects near threshold. It stems from recent developments in nanotechnology, which allow one to obtain a strictly two–dimensional electron gas subject to confined geometries [11,12]. To be definite, we shall consider the device of Figure 1, where a resonant cavity or stub having width c and length l_s is coupled to a uniform guide of indefinite length and width b. The stub contains a region, depicted by the shaded area in Figure 1, with a defect described by a potential field $V(x,y)$. For high–purity materials and at low temperatures, the electron's motion inside the duct is ballistic, and can be described as a scattering process [11,12], the conductivity of the quantum circuit being expressible in term of the transmission coefficients of the system. Recently, we have developed an S–matrix approach to stubbed wave guides with defects, which allows for an accurate numerical solution of the scattering problem even when some critical dimension of the system gets large [13]. We start from the two–dimensional Schrödinger equation

$$\left\{-\frac{\hbar^2}{2m^*}\nabla_2^2 + V(x,y)\right\}\Psi(x,y) = E\Psi(x,y), \qquad (2)$$

where ∇_2^2 is the two–dimensional Laplace operator, E the total energy, and m^* represents the effective mass of the electron in the conduction band. For real energies, the Schrödinger equation (2) is solved, with the boundary condition that $\Psi(x,y)$ vanishes along the boundaries of the device, by piecewise expanding the total wave function into a complete set of transverse-mode eigenfunctions, i.e.,

$$\Psi^{(i)}(x,y) = \sum_n \psi_n^{(i)}(x)\phi_n^{(i)}(y) \quad i = 1,\ldots,5. \qquad (3)$$

In writing the expansion (3) we have taken into account that the whole system can be divided into five regions; the leads, the two cavities in the sidearm where there is no defect, and the region where the potential acts. If hard–wall boundary conditions are assumed, the transverse modes are described by the eigenfunctions of an infinite square well having width b in the leads, and width c in the empty regions of the stub. In presence of the potential, namely for $x_2 \le x \le x_3$, the basis functions can be expressed as linear combinations of the infinite–well eigenfunctions provided that the potential has the simple form

$$V(x,y) = V_0 f(y)\Theta(x - x_0)\Theta(x_f - x), \qquad (4)$$

where $\Theta(x - x_r)$ is the Heaviside step function. Indeed, in such a case one has just to diagonalize the Hamiltonian $\mathcal{H}(x) = -\frac{\hbar^2}{2m^*}\frac{d^2}{dy^2} + V_0 f(y)$ for the transverse motion, in the model space spanned by the infinite–well wave functions. By means of the expansion (3), the Schrödinger equation is transformed into an (in principle) infinite set of uncoupled, one–dimensional differential equations for the expansion coefficients $\psi_n^{(i)}(x)$. These coefficients can be written in terms of forward and backward propagating waves. For instance, in the lead on the left-hand side one gets

$$\psi_n^{(1)}(x) = \overrightarrow{c}_n^{(1)} e^{ik_n^{(l)}(x-x_1)} + \overleftarrow{c}_n^{(1)} e^{-ik_n^{(l)}(x-x_1)}. \qquad (5)$$

Here, the wave numbers $k_n^{(l)}$ are given by

$$k_n^{(l)} = \sqrt{\frac{2m^*}{\hbar^2}E - \left(\frac{n\pi}{b}\right)^2} \equiv \sqrt{\frac{2m^*\left(E - \epsilon_n^{(l)}\right)}{\hbar^2}}, \qquad (6)$$

for $E > \epsilon_n^{(l)}$, i.e., for an energetically allowed mode, and by

$$k_n^{(l)} = i\kappa_n^{(l)} \equiv i\sqrt{\left(\frac{n\pi}{b}\right)^2 - \frac{2m^*}{\hbar^2}E} \qquad (7)$$

for a closed channel, where the wave function is exponentially damped in the waveguide [13]. Similar considerations apply in the other regions of the device; in the lead on the right–hand–side one has the same wave numbers $k_n^{(l)}$ as on the left, while in the empty cavities the propagation wave numbers are given by equations (6) and (7) with the width b of the waveguide replaced by the stub's transverse dimension c. Finally, in the defect region the transverse eigenvalues $\epsilon_n^{(l)}$ have to be replaced by the eigenvalues $\mathcal{E}_n$ of the transverse Hamiltonian $\mathcal{H}(x)$.

The forward and backward amplitudes $\overrightarrow{c}_n^{(i)}$ and $\overleftarrow{c}_n^{(i)}$ in the various regions of the device can be finally related to one another matching the wave function and its first derivative at the interfaces delimiting the ducts from the cavity, and the empty parts of the cavity from the region where the potential acts. Once the amplitudes of the waves leaving an interface are expressed in terms of the amplitudes of the incoming waves, the scattering operator for each segment in the quantum circuit can be evaluated through linear algebra. The total S–matrix of the stubbed waveguide is finally obtained from the partial scattering operators by recursively applying the $\star$-product composition rule, which expresses the overall scattering matrix $\mathbf{S}$ in terms of the partial scattering matrices $\mathbf{S}^{(a)}$ and $\mathbf{S}^{(b)}$ referring to two subsystems a and b, as [11,13]

$$\mathbf{S} = \begin{pmatrix} \mathbf{S}_{11} & \mathbf{S}_{12} \\ \mathbf{S}_{21} & \mathbf{S}_{22} \end{pmatrix} = \mathbf{S}^{(a)} \bigstar \mathbf{S}^{(b)}, \qquad (8)$$

where

$$\mathbf{S}_{11} = \mathbf{S}_{11}^{(a)} + \mathbf{S}_{12}^{(a)}\mathbf{S}_{11}^{(b)}\left(\mathbf{1} - \mathbf{S}_{22}^{(a)}\mathbf{S}_{11}^{(b)}\right)^{-1}\mathbf{S}_{21}^{(a)}, \quad (9a)$$

$$\mathbf{S}_{12} = \mathbf{S}_{12}^{(a)}\left(\mathbf{1} - \mathbf{S}_{11}^{(b)}\mathbf{S}_{22}^{(a)}\right)^{-1}\mathbf{S}_{12}^{(b)}, \quad (9b)$$

$$\mathbf{S}_{21} = \mathbf{S}_{21}^{(b)}\left(\mathbf{1} - \mathbf{S}_{22}^{(a)}\mathbf{S}_{11}^{(b)}\right)^{-1}\mathbf{S}_{21}^{(a)}, \quad (9c)$$

$$\mathbf{S}_{22} = \mathbf{S}_{22}^{(b)} + \mathbf{S}_{21}^{(b)}\mathbf{S}_{22}^{(a)}\left(\mathbf{1} - \mathbf{S}_{11}^{(b)}\mathbf{S}_{22}^{(a)}\right)^{-1}\mathbf{S}_{12}^{(b)}. \quad (9d)$$

In the present case two types of partial scattering matrices occur; (a) the S–matrices $\mathbf{S}(x_i)$ $(i = 1, 4)$ which describe the scattering of the wave function at the waveguide/stub discontinuities or its propagation into and out the defect potential; (b) the scattering operators associated to the propagation of the electron's wave along each segment of the device. As discussed at length in [13], it is a distinctive feature of the scattering matrix that it is numerically stable also for "large" systems. Moreover, the composition rule (8) naturally accommodates a different number of modes in the lead and in the cavity. These features are of particular relevance in the present instance, where the stub's width c may vary over a rather large range of values.

It is worth to stress here that each block $\mathbf{S}_{ij}$ in the scattering operator $\mathbf{S}$ is itself a matrix, whose elements are labeled by mode or channel indexes. For an incoming wave of unit flux impinging from the left, $(\mathbf{S}_{11})_{nm}$ represents the reflection coefficient towards the left from the initial channel m into the final one n, whereas $(\mathbf{S}_{21})_{nm}$ is the transmission coefficient to the right from mode m into mode n. Similarly, $(\mathbf{S}_{12})_{nm}$ and $(\mathbf{S}_{22})_{nm}$ are the $m \to n$ transmission amplitudes to the left and reflection coefficient to the right for an electron incoming from the right. Once the transmission coefficients are known, the total conductance G (in units $2e^2/h$) is given by the Büttiker formula [11,12,14]

$$G = \sum_{m,n} \frac{k_n^{(l)}}{k_m^{(l)}} \left|(\mathbf{S}_{21})_{nm}\right|^2, \quad (10)$$

where the sum is restricted to the open channels in the duct.

The above S–matrix approach can be straightforwardly extended to complex energies and complex channel momenta to numerically locate the poles of the S–matrix on the multi–sheeted energy surface. In the following, sheets will be specified according to the sign of the imaginary part of the lead momenta in the various channels [15,16]. Thus, for a four–channel situation, the physical sheet, where all the imaginary parts of the momenta are positive, will be denoted as $(++++)$, whereas on the sheet $(-+++)$ one has $\mathrm{Im}\, k_1^{(l)} < 0$ and $\mathrm{Im}\, k_i^{(l)} > 0$ for the other three channels. On this sheet, one is looking for solutions of the Schrödinger equation with outgoing components which diverge exponentially for $x \to -\infty$ and $x \to +\infty$ in the elastic channel, whereas they are exponentially damped in the other channels. A pole at $E = E_p \equiv E^{(R)} - i\Gamma$ in the fourth quadrant of this sheet near the real energy axis produces resonance effects in the conductance G provided that its real part is in between the first and second scattering thresholds $\epsilon_1^{(l)}$ and $\epsilon_2^{(l)}$. In other words, if $\epsilon_1^{(l)} \le E^{(R)} \le \epsilon_2^{(l)}$ one observes a peak or dip in the conductance around $E \sim E^{(R)}$, with width 2Γ. Such a pole is referred to as being dominant. Similarly, dominant poles for resonances in the second subband at physical energies in between $\epsilon_2^{(l)}$ and $\epsilon_3^{(l)}$ lie in sheet $(--++)$ and have $\epsilon_2^{(l)} \le E^{(R)} \le \epsilon_3^{(l)}$. The poles, which are expected to occur in all the S–matrix elements, have been located numerically in the energy plane by looking for the zeroes of $\mathcal{I} \equiv |\,(\mathbf{S}_{21})_{11}\,|^{-1}$. We verified, however, that the same results are obtained starting from a different matrix element of $\mathbf{S}$. Since a direct solution of the equation $\mathcal{I} = 0$ would have been quite cumbersome, we actually searched for the minima of $\mathcal{I}$ in the various sheets of the energy Riemann surface. We have chosen the value $m^* = 0.067 m_e$ for the effective electron mass, which is appropriate for the $Al_xGa_{1-x}As/GaAs$ interface. We verified that convergence is attained for both the conductance and the pole positions when four channels are included in the external duct, and up to ten channels are taken into account in the cavity. In these conditions, the position of the poles in the complex energy plane can be guaranteed with an accuracy of the order 10^{-5}. From now on, to exploit the scale invariance of the system, all lengths are measured in terms of the waveguide width b, and energies in terms of the waveguide fundamental mode $\epsilon_1^{(l)} = \frac{\hbar^2}{2m^*}\left(\frac{\pi}{b}\right)^2$, and the "tilde" symbol will be used to denote adimensional quantities. Thus, the various thresholds $\epsilon_n^{(l)} = n^2\epsilon_1^{(l)}$ will become simply $\tilde{\epsilon}_n^{(l)} = 1, 4, 9, \ldots$ The calculations we present refer to a device with $\tilde{l}_s \equiv l_s/b = 1$; a double Gaussian defect

$$\tilde{V}(\tilde{x}, \tilde{y}) \equiv \tilde{V}_0 e^{-\tilde{\beta}^2(\tilde{x}-\tilde{x}_c)^2 - \tilde{\alpha}^2(\tilde{y}-\tilde{y}_c)^2} \quad (11)$$

centered in $(\tilde{x}_c, \tilde{y}_c) = (0.50, 0.25)$ has been allowed in the cavity. The decay constants along the transverse and propagation direction have been fixed at $\tilde{\alpha} \equiv \alpha b = 15$, $\tilde{\beta} \equiv \beta b = 10$, respectively. This choice ensures that the potential is entirely contained within a region $\tilde{w} = 0.3$ wide and $\tilde{l}_d = 1$ long. Moreover, we consider a displacement $\tilde{Y}_0 = 0.1$ of the defect area from the lower edge of the guide. The smooth dependence of $\tilde{V}(\tilde{x}, \tilde{y})$ has been taken into account through a slicing technique, i.e., replacing the actual interaction with a sequence of N pseudo-defects satisfying equation (4); each of them has a constant value $\tilde{V}_0(j) = \exp\left(-\tilde{\beta}^2(\tilde{x}_j - \tilde{x}_c)^2\right)$ $(j = 1, \ldots, N)$ along the x direction and a Gaussian profile in the transverse direction [13,17]. Quite stable results are obtained with $N = 10 \div 15$ slices. In the present calculations we have chosen $\tilde{V}_0 = 4$.

In Figure 2 we report the trajectories on the complex energy surface of three S–matrix poles with varying stub's width $\tilde{c}$. Pole 1 moves from the upper edge $\tilde{\epsilon}_2^{(l)}$ towards the lower edge $\tilde{\epsilon}_1^{(l)}$ of the first subband as $\tilde{c}$ is increased from 1.50 to 5.00. Similarly, pole 2 moves downwards from the third threshold passing below the second one as $\tilde{c}$ is increased from $\tilde{c} = 1.00$ up to $\tilde{c} = 2.00$, whereas pole 3

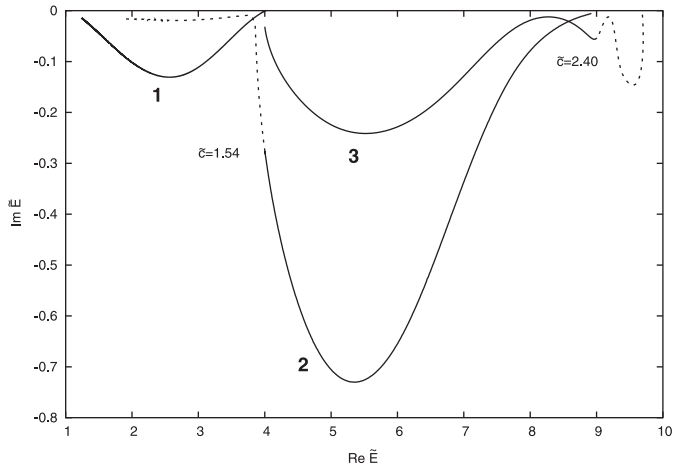

Fig. 2. Motion of three S–matrix poles on the Riemann energy surface with varying $\tilde{c}$. The three trajectories correspond to $1.50 \leq \tilde{c} \leq 5.00$, $1.00 \leq \tilde{c} \leq 2.00$, and $1.33 \leq \tilde{c} \leq 5.00$ for pole 1, 2, and 3, respectively. The poles move from right to left as $\tilde{c}$ increases. Note that pole 1 is on the $(-++)$ sheet, whereas poles 2 and 3 belong to the $(--+)$ sheet. Shadow and dominant poles are drawn as dashed and full lines, respectively. The values of $\tilde{c}$ where a pole changes its nature are given in the figure.

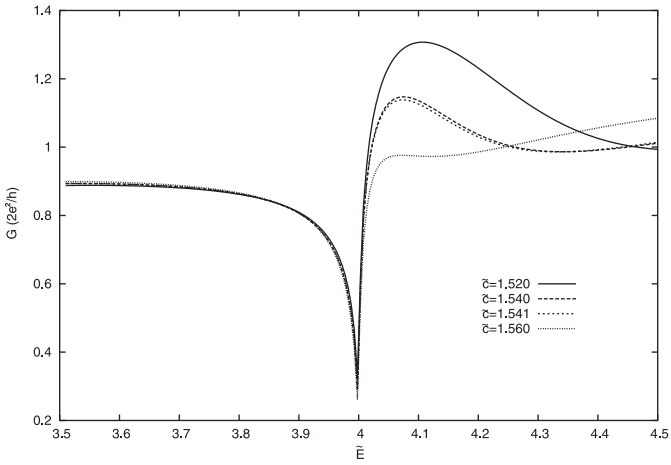

Fig. 3. Conductance (in units $2e^2/h$) in the region of the second threshold for $\tilde{c} = 1.520$ (solid line), $\tilde{c} = 1.540$ (dashed line), $\tilde{c} = 1.541$ (short–dashed line), and $\tilde{c} = 1.560$ (dotted line).

refer to $1.33 \leq \tilde{c} \leq 5.00$. In all cases one has the "binding" effect typical of an increase of the stub's width [13]. Note that the three pole trajectories appear to be close to each other, but are in fact on different sheets of the energy Riemann surface. Pole 1 lies on the $(-+++)$ sheet, and can produce resonance effects in the first subband, whereas poles 2 and 3 belong to the $(--++)$ sheet, and are responsible of resonance structures in the second subband. As a consequence, pole 2 is a dominant pole until it passes below $\tilde{\epsilon}_2^{(l)}$, which happens for $\tilde{c} = 1.54$; for $\tilde{c} > 1.54$ it becomes a shadow pole, since the $(--++)$ sheet is more distant from the first subband than the $(-+++)$ sheet, where the relevant resonance poles may be found. Similarly, pole 3 is shadow for $\tilde{c} < 2.40$, and becomes a dominant pole for greater values of $\tilde{c}$. In Figure 2 the dominant or shadow status of poles is exhibited with full and dashed lines, respectively.

The change of status of a pole from dominant to shadow pole as it passes a threshold can explain the remarkable effects that even small variations of $\tilde{c}$ may have on the conductance near threshold. This is illustrated in Figure 3, where we plot the conductance for real energies around the second threshold ($3.5 \leq \tilde{E} \leq 4.5$), in correspondence to $\tilde{c} = 1.520$, 1.540, 1.541, and 1.560. The corresponding conductance profiles are given by the solid, long–dashed, short-dashed, and dotted lines, respectively.

For $\tilde{c} = 1.520$ pole 2 is dominant, since one has $\tilde{E}_p \simeq 4.14 - 0.39i$, and produces the resonance peak one observes just above threshold. For $\tilde{c} = 1.540$ and $\tilde{c} = 1.541$ pole 2 is just above ($\tilde{E}_p \simeq 4.002 - 0.276i$) and just below ($\tilde{E}_p \simeq 3.990 - 0.270i$) the second threshold, respectively. One has that the resonance peak is still visible in both cases, which means that the dominant $\rightarrow$ shadow transition does not prevent the pole from having effects on the observable quantities. For $\tilde{c} = 1.560$ the pole has moved down to $\tilde{E}_p \simeq 3.870 - 0.090i$, and it is far away enough from the physical region, to have no effects on the conductance, which appears rather flat above threshold. It is worth to stress that for these values of $\tilde{c}$ pole 1 is far above the second threshold, and cannot influence the conductance profile in the first subband; as a matter of fact, in all cases the conductance is practically the same below threshold, and exhibits a cusp structure, with infinite slope as a function of energy both from above and from below. This behavior is indeed discernible at threshold in all calculations, and can be explained much in the same way, as one explains threshold phenomena in inelastic scattering processes. When a new transverse mode opens up, less energy is available in the propagation direction, so that one has the analogue of "endoergic" reactions in inelastic scattering [3]. From equation (10) one sees that G is linear with respect to the corresponding final momentum $k_n^{(l)}$. Since $k_n^{(l)}$ is related to the total energy E and to the relevant waveguide eigenenergy $\epsilon_n^{(l)}$ by equation (6), one actually expects an infinite derivative of G with respect to E [3].

The effects due to the exchange of role between shadow and dominant poles are illustrated in Figure 4, where we plot G near the second threshold for $\tilde{c} = 1.54$ (solid line) and $\tilde{c} = 1.70$ (dashed line). In the former case one has the resonance peak above threshold due to pole 2, as discussed previously; in the latter, pole 2 has moved down to $\tilde{E}_p \simeq 2.680 - 0.020i$ and has no effect on the conductance any longer; pole 1 which moves on the $(-+++)$ sheet, on the other hand, is now dominant, being located at $\tilde{E}_p \simeq 3.780 - 0.020i$, and produces the Fano dip one observes in Figure 4. Note that in the first subband one can have the simultaneous presence of poles and transmission zeros, which cannot occur when more than a propagating mode are active.

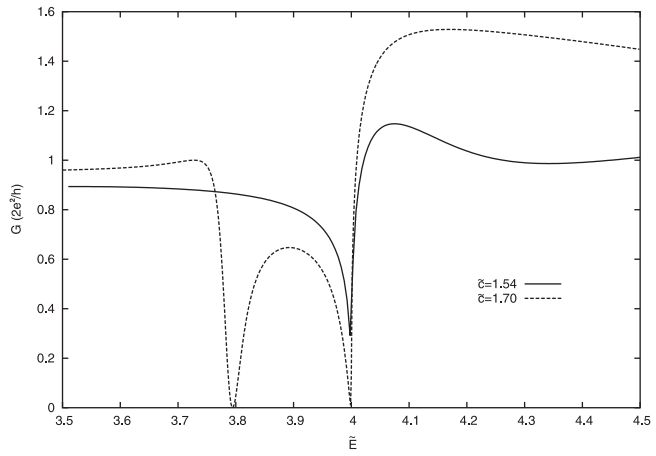

Fig. 4. Conductance (in units $2e^2/h$) in the region of the second threshold for $\tilde{c} = 1.54$ (solid line) and $\tilde{c} = 1.70$ (dashed line).

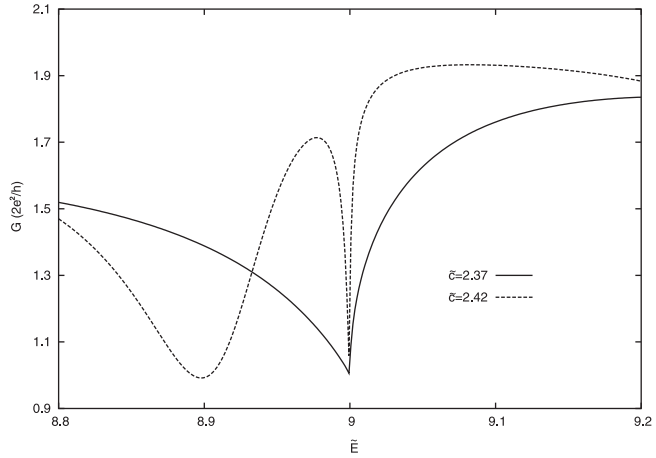

Fig. 5. Conductance (in units $2e^2/h$) in the region of the third threshold for $\tilde{c} = 2.37$ (solid line) and $\tilde{c} = 2.42$ (dashed line).

A similar phenomenon is visible in correspondence to the third threshold. An example is given in Figure 5, where the conductance around the third threshold is plotted for $\tilde{c} = 2.37$ and $\tilde{c} = 2.42$. While a resonance dip is clearly visible in the latter case, no resonance at all is discernible for the shorter stub, and only the threshold cusp survives for the conductance profile. Such a striking change in correspondence to so small a change in the cavity width can be readily explained in terms of a dominant to shadow pole transition. Indeed, for $\tilde{c} = 2.42$ pole 3 of Figure 2 is located at $\tilde{E}_p \simeq 8.920 - 0.053i$ in the $(--++)$ sheet, and plays the role of dominant pole for the second subband. When the stub is shortened, the pole moves on its sheet up to $\tilde{E}_p \simeq 9.110 - 0.023i$, in correspondence to the third subband, and becomes a shadow pole.

In conclusion, we have demonstrated that the behavior of the conductance near the thresholds for the opening of new propagating modes, and its sometimes striking changes in correspondence to moderate or even small variations of the stub's width are signals of the transition from a dominant to a shadow status of the S–matrix poles. This result shows that concepts and methods of the analytic S–matrix, widely employed in traditional scattering theory, may have their counterpart in the analysis of systems with a confined geometry.

References

1. R.J. Eden, P.V. Landshoff, D.I. Olive, J.C. Polkinghorne, *The Analytic S–Matrix* (Cambridge University Press, Cambridge, 1966)
2. H.M. Nussenzveig, *Causality and Dispersion Relations* (Academic Press, New York, 1972)
3. R.G. Newton, *Scattering Theory of Waves and Particles* (Springer, New York, 1982)
4. N. Moiseyev, Phys. Rep. **302**, 211 (1998)
5. R.J. Eden, J.R. Taylor, Phys. Rev. B **133**, 1575 (1964)
6. Y. Fujii, M. Fukugita, Nucl. Phys. B **85**, 179 (1975)
7. R.E. Brown, N. Jarmie, G.M. Hale, Phys. Rev. C **35**, 1999 (1987)
8. A. Herzenberg, D. Ton-That, J. Phys. B **8**, 426 (1975)
9. R.M. Potvliege, R. Shakeshaft, Phys. Rev. A **38**, 6190 (1988)
10. M. Dörr, R.M. Potvliege, Phys. Rev. A **41**, 1472 (1990)
11. S. Datta, *Electronic Transport in Mesoscopic Systems* (Cambridge University Press, Cambridge, 1995)
12. D.K. Ferry, S.M. Goodnick, *Transport in Nanostructures* (Cambridge University Press, Cambridge, 1997)
13. G. Cattapan, P. Lotti, Eur. Phys. J. B **60**, ??? (2007)
14. R. Büttiker, Y. Imry, R. Landauer, S. Pinhas, Phys. Rev. B **31**, 6207 (1985)
15. R.K. Logan, H.W. Wild, Phys. Rev. **158**, 1467 (1967)
16. A.M. Badalyan, L.P. Kok, M.I. Polikarpov, Yu.A. Simonov, Phys. Rep. **82**, 31 (1982)
17. W.-D. Sheng, J.-B. Xia, J. Phys.: Condens. Matter **8**, 3635 (1996)